Publication Year	2017
Acceptance in OA	2021-01-07T11:24:19Z
Title	AGILE Observations of the Gravitational-wave Source GW170817: Constraining Gamma-Ray Emission from an NS-NS Coalescence
Authors	VERRECCHIA, Francesco, TAVANI, MARCO, Donnarumma, I., BULGARELLI, ANDREA, EVANGELISTA, YURI, PACCIANI, LUIGI, URSI, ALESSANDRO, PIANO, Giovanni, PILIA, Maura, CARDILLO , MARTINA, PARMIGGIANI, NICOLO, GIULIANI, ANDREA, PITTORI, Carlotta, Longo, F., LUCARELLI, Fabrizio, MINERVINI, GABRIELE, FEROCI, MARCO, ARGAN, ANDREA, FUSCHINO, FABIO, LABANTI, CLAUDIO, Marisaldi, M., FIORETTI, VALENTINA, TROIS, ALESSIO, DEL MONTE, Ettore, ANTONELLI, Lucio Angelo, Barbiellini, G., CARAVEO, PATRIZIA, Cattaneo, P. W., Colafrancesco, S., Costa, E., D'Amico, F., Ferrari, A., Giommi, P., Morselli, A., Paoletti, F., PELLIZZONI, ALBERTO PAOLO, Picozza, P., Rappoldi, A., SOFFITTA, PAOLO, VERCELLONE, STEFANO, Baroncelli, L., Zollino, G.
Publisher's version (DOI)	10.3847/2041-8213/aa965d
Handle	http://hdl.handle.net/20.500.12386/29524
Journal	THE ASTROPHYSICAL JOURNAL LETTERS
Volume	850

The Astrophysical Journal Letters, 850:L27 (9pp), 2017 December 1 https://doi.org/10.3847/2041-8213/aa965d

AGILE Observations of the Gravitational-wave Source GW170817: Constraining Gamma-Ray Emission from an NS–NS Coalescence

F. Verrecchia[1,2], M. Tavani[3,4,5], I. Donnarumma[6,3], A. Bulgarelli[7], Y. Evangelista[3], L. Pacciani[3], A. Ursi[3], G. Piano[3], M. Pilia[8], M. Cardillo[3], N. Parmiggiani[7], A. Giuliani[9], C. Pittori[1,2], F. Longo[10], F. Lucarelli[1,2], G. Minervini[3], M. Feroci[3], A. Argan[3], F. Fuschino[7], C. Labanti[7], M. Marisaldi[11], V. Fioretti[7], A. Trois[8], E. Del Monte[3], L. A. Antonelli[1], G. Barbiellini[10], P. Caraveo[9], P. W. Cattaneo[12], S. Colafrancesco[13], E. Costa[3,6], F. D'Amico[6], A. Ferrari[14], P. Giommi[6], A. Morselli[15], F. Paoletti[11,3], A. Pellizzoni[8], P. Picozza[15], A. Rappoldi[12], P. Soffitta[3], S. Vercellone[16], L. Baroncelli[7], and G. Zollino[7]
[1] Space Science Data Center/ASI (SSDC), via del Politecnico, I-00133 Roma, Italy
[2] INAF-OAR, via Frascati 33, I-00078 Monte Porzio Catone (Roma), Italy
[3] INAF-IAPS, via del Fosso del Cavaliere 100, I-00133 Roma, Italy
[4] Dipartimento di Fisica, Università di Roma "Tor Vergata", via della Ricerca Scientifica 1, I-00133 Roma, Italy
[5] Gran Sasso Science Institute, viale Francesco Crispi 7, I-67100 L'Aquila, Italy
[6] ASI, via del Politecnico snc, I-00133 Roma, Italy
[7] INAF-IASF-Bologna, via Gobetti 101, I-40129 Bologna, Italy
[8] INAF, Osservatorio Astronomico di Cagliari, via della Scienza 5, I-09047 Selargius (CA), Italy
[9] INAF-IASF Milano, via E.Bassini 15, I-20133 Milano, Italy
[10] Dipartimento di Fisica, Università di Trieste and INFN, via Valerio 2, I-34127 Trieste, Italy
[11] Birkeland Centre for Space Science, Department of Physics and Technology, University of Bergen, Bergen, Norway
[12] INFN–Pavia, via Bassi 6, I-27100 Pavia, Italy
[13] University of Witwatersrand, Johannesburg, South Africa
[14] CIFS, c/o Physics Department, University of Turin, via P. Giuria 1, I-10125 Torino, Italy
[15] INFN–Roma Tor Vergata, via della Ricerca Scientifica 1, I-00133 Roma, Italy
[16] INAF, Osservatorio Astronomico di Brera, via Emilio Bianchi 46, I-23807 Merate (LC), Italy
Received 2017 October 13; revised 2017 October 25; accepted 2017 October 25; published 2017 November 27

Abstract

The LIGO–Virgo Collaboration (LVC) detected, on 2017 August 17, an exceptional gravitational-wave (GW) event temporally consistent within ∼1.7 s with the GRB 1708117A observed by *Fermi*-GBM and *INTEGRAL*. The event turns out to be compatible with a neutron star–neutron star (NS–NS) coalescence that subsequently produced a radio/optical/X-ray transient detected at later times. We report the main results of the observations by the *AGILE* satellite of the GW170817 localization region (LR) and its electromagnetic (EM) counterpart. At the LVC detection time T_0, the GW170817 LR was occulted by the Earth. The *AGILE* instrument collected useful data before and after the GW/GRB event because in its spinning observation mode it can scan a given source many times per hour. The earliest exposure of the GW170817 LR by the gamma-ray imaging detector started about 935 s after T_0. No significant X-ray or gamma-ray emission was detected from the LR that was repeatedly exposed over timescales of minutes, hours, and days before and after GW170817, also considering Mini-calorimeter and Super-*AGILE* data. Our measurements are among the earliest ones obtained by space satellites on GW170817 and provide useful constraints on the precursor and delayed emission properties of the NS–NS coalescence event. We can exclude with high confidence the existence of an X-ray/gamma-ray emitting magnetar-like object with a large magnetic field of 10^{15} G. Our data are particularly significant during the early stage of evolution of the EM remnant.

Key words: gravitational waves – gamma rays: general

1. Introduction

Automatic processing of *Fermi*-GBM data revealed, on 2017 August 17, a low-fluence short gamma-ray burst (GRB; now named GRB 170817A) detected in the 10–1000 keV range (Connaughton et al. 2017; Goldstein et al. 2017) with a public notice emitted seconds after the event trigger (von Kienlin et al. 2017). The LIGO–Virgo Collaboration (LVC) identified a very significant gravitational-wave (GW) event preceding the GBM trigger by 1.7 s. Rapid communication of this double event was promptly issued (LIGO Scientific Collaboration & Virgo Collaboration 2017a, 2017b, 2017c, 2017d, 2017e). GRB 170817A was soon confirmed by *INTEGRAL*/SPI-ACS (Savchenko et al. 2017a; V. Savchenko et al. 2017, in preparation; Abbott et al. 2017e). This event (now named GW170817) is relevant for several reasons. It is the first GW source detected in close temporal coincidence with a short GRB, suggesting a physical relation between the two events. It is the first detected gravitational-wave event associated with a coalescence of two neutron stars. Furthermore, it is the second GW event for which Advanced Virgo (Acernese et al. 2015) could provide crucial constraints on the localization region restricting it to a few tens of square degrees. These remarkable facts allowed the scientific community, for the first time, to search for counterparts in an effective way (Abbott et al. 2017d, hereafter MMA17).

The GW event occurred at time $T_0 = 12{:}41{:}04.446$ UTC (Abbott et al. 2017b, hereafter A17b). The event was identified by LVC as a compact binary coalescence (CBC) of two neutron stars (NSs) of total mass $2.82^{+0.47}_{-0.09}\ M_\odot$ and individual masses in the range 0.86–2.26 $M_\odot$. The estimated redshift of the system is $z = 0.008^{+0.002}_{-0.003}$ corresponding to a distance of 40 ± 8 Mpc (A17b). GW170817 is the first NS star coalescence candidate event with a "false-alarm rate" (FAR) less than one in

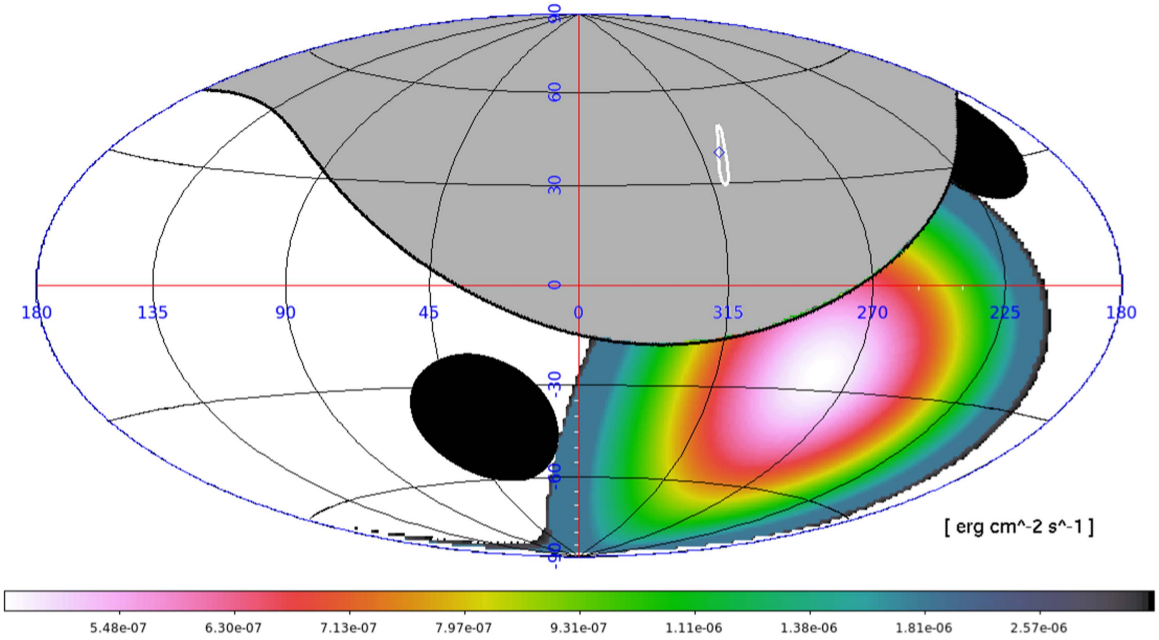

Figure 1. *AGILE*-GRID $E > 30$ MeV UL map (in erg cm^{-2} s^{-1} and Galactic coordinates) based on the gamma-ray 4 s exposure at the detection time T_0 of GW170817. The shadowed areas show the Earth-occulted region and the sky fraction not directly accessible by *AGILE* for solar panel constraints. The white contour shows the "preliminary LAL-inference" 90% c.l. LR of GW170817 (LIGO Scientific Collaboration & Virgo Collaboration 2017e) and the blue diamond marker is at the OT AT 2017gfo position. The *AGILE* instrument does not have significant exposure of the LR at T_0, which is covered by the Earth contour.

8.0×10^4 years as determined by a refined analysis (A17b). This event is the fifth of a set of confirmed GW events detected by LVC, GW150914 and GW151226 (Abbott et al. 2016a, 2016b, 2016c, 2016d, 2016e, 2016f), GW170104 (Abbott et al. 2017a), and the more recent GW170814 (Abbott et al. 2017c), the first revealed using the Virgo detector data.

A first sky map of GW170817 was distributed through a LVC-GCN on 2017 August 17 (LIGO Scientific Collaboration & Virgo Collaboration 2017b), including an initial localization generated by the BAYESTAR pipeline (Singer & Price 2016) and based on data from the LIGO Hanford data only. An updated sky map was distributed about 10 hr later (LIGO Scientific Collaboration & Virgo Collaboration 2017e), obtained using LAL-Inference (Veitch et al. 2015), based on data from the three detectors LIGO Hanford, LIGO Livingston, and Virgo. The source could be located in a sky region of 28 deg^2 (90% c.l.).

After the LVC announcement, a multi-wavelength campaign immediately started. The campaign involved the X-ray and gamma-ray satellites first, and radio/IR–optical/TeV ground observatories at later times. The detection of a new optical transient (OT) was first announced by the One-meter, Two-hemisphere (1M2H) team discovered with the 1 m Swope telescope on August 18 01:05 UT (Coulter et al. 2017a, 2017b; Drout et al. 2017), named Swope Supernova Survey 2017a (SSS17a, now with the IAU designation AT 2017gfo). The OT was also detected independently by five other teams, the Dark Energy Camera (Allam et al. 2017; Cowperthwaite et al. 2017), the Distance Less Than 40 Mpc Survey (L. Tartaglia et al. 2017, in preparation; Valenti et al. 2017; Yang et al. 2017), Las Cumbres Observatory (Arcavi et al. 2017a, 2017b, 2017c), the Visible and Infrared Survey Telescope for Astronomy (Tanvir et al. 2017a, 2017b), and MASTER (Lipunov et al. 2017b, 2017a), REM-ROS2 (Melandri et al. 2017; Pian et al. 2017a, 2017b), *Swift* UVOT/XRT (Evans et al. 2017b, 2017a), and Gemini-South (Kasliwal et al. 2017; Singer et al. 2017), and for all see also MMA17. AT 2017gfo is located at 10.″6 from the early-type galaxy NGC 4993, at a distance of ∼40 Mpc. A sequence of satellite high-energy observations started almost immediately, with exposures of the GW170817 LR depending on satellite position and operations. The X-ray and γ-ray observations included contributions by *CALET* (Nakahira et al. 2017), *Konus-Wind* (Svinkin et al. 2017), *Insight-HXMT* (Li et al. 2017; Liao et al. 2017), *AstroSat* CZTI (Balasubramanian et al. 2017), *AGILE*-GRID (see below), *Fermi*-LAT (Kocevski et al. 2017), *MAXI* (Sugita et al. 2017; S. Sugita et al. 2017, in preparation), Super-*AGILE* (MMA17; this work), *Swift* X-ray Telescope (Evans et al. 2017b, 2017a), *NuSTAR* (Harrison et al. 2017), *INTEGRAL* JEM-X (Savchenko et al. 2017b; V. Savchenko et al. 2017, in preparation), and *Chandra* (Fong et al. 2017; Margutti et al. 2017a; Troja et al. 2017b). An X-ray counterpart detection at the OT position was reported after 9 days and confirmed after 15 days by *Chandra* (Fong et al. 2017; Margutti et al. 2017b; Troja et al. 2017a, 2017b). Moreover, an important detection in the radio band has been reported by VLA (Alexander et al. 2017a, 2017b).

AGILE promptly reacted to the initial LVC notification of GW170817 and started a quicklook analysis as data became available within 1–2 hr as discussed below (Bulgarelli et al. 2017; Piano et al. 2017; Pilia et al. 2017; Verrecchia et al. 2017).

The *AGILE* satellite that is in an equatorial orbit at an altitude of ∼500 km (Tavani et al. 2009) is exposing 80% of the entire sky every 7 minutes in a "spinning mode," with an instantaneous field of view (FoV) of a radius of 70°. The instrument consists of an imaging gamma-ray Silicon Tracker (sensitive in the energy range 30 MeV–30 GeV), Super-*AGILE* (SA; operating in the energy range 20–60 keV), and the Mini-calorimeter (MCAL; working in the range 0.35–100 MeV; Fuschino et al. 2008; Marisaldi et al. 2008; Labanti et al. 2009) with an omni-directional FoV and self-triggering capability in burst mode for various trigger

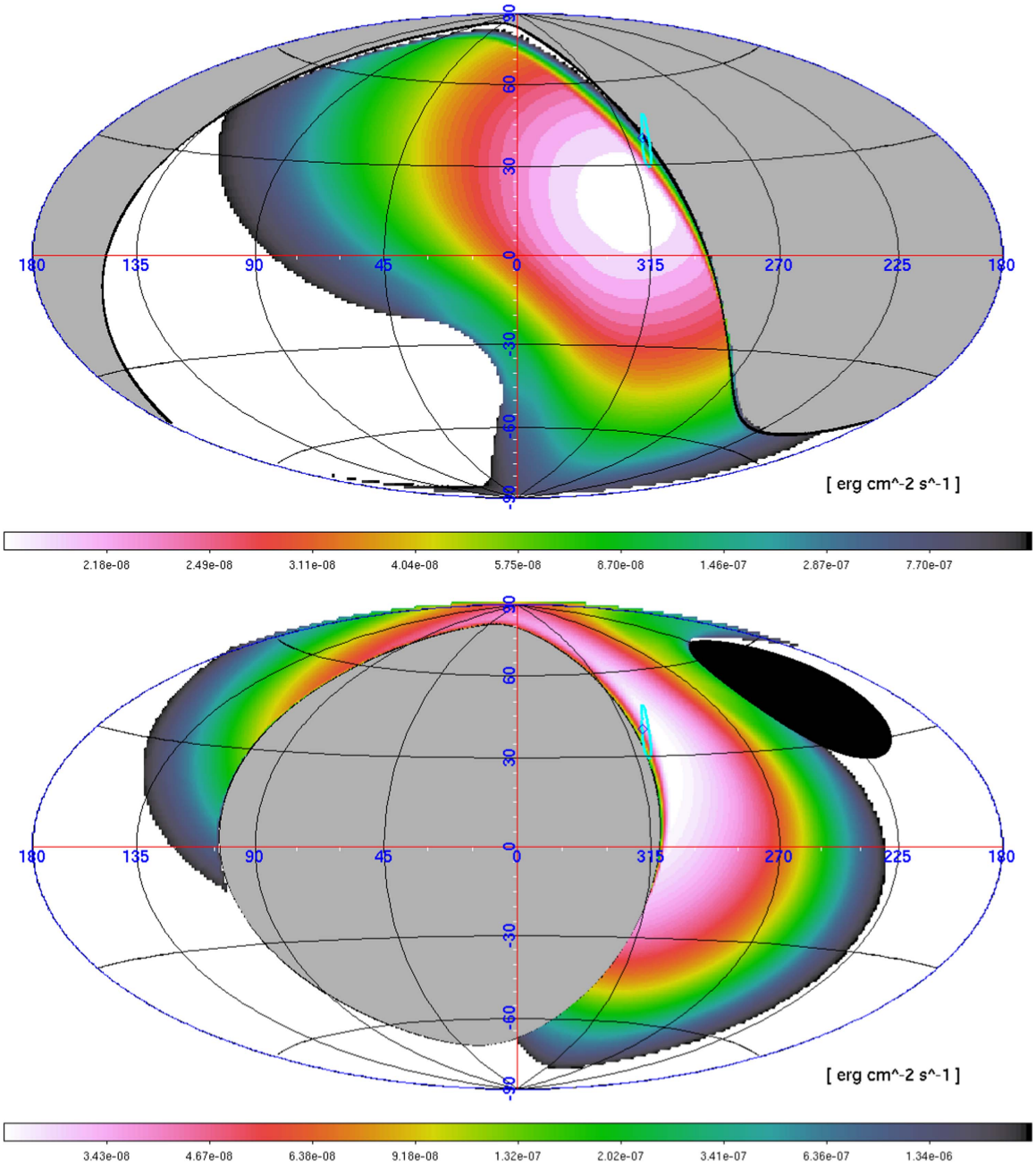

Figure 2. *AGILE*-GRID $E > 30$ MeV UL maps (in erg cm^{-2} s^{-1} and Galactic coordinates) for the 150 s exposures nearest to the T_0, centered at -1260 and $+1010$ s (times refers to T_0). The "preliminary LAL-inference" 90% c.l. LR of GW170817 (LIGO Scientific Collaboration & Virgo Collaboration 2017e) is shown in cyan color, and the blue diamond marker is at the optical transient AT 2017gfo position.

timescales. The anti-coincidence (AC) system completes the instrument (for a summary of the *AGILE* mission features, see Tavani et al. 2009). The combination of Tracker, MCAL, and AC working as a gamma-ray imager constitutes the *AGILE*-GRID. The instrument is capable of detecting gamma-ray transients and GRB-like phenomena on timescales ranging from submilliseconds to tens–hundreds of seconds.

The *AGILE* instrument has important characteristics for observations of large GW source LRs: a very large FoV of the GRID (2.5 sr); 80% of the whole sky that can be exposed every 7 minutes; 100–150 useful passes every day for any region in the accessible sky; a gamma-ray exposure of ~ 2 minutes of any field in the accessible sky every 7 minutes; sensitivity of $\sim 10^{-8}$ erg cm^{-2} s^{-1} above 30 MeV for typical single-pass of unocculted sky regions; a submillisecond MCAL trigger for very fast events in the range 0.4–100 MeV; hard X-ray (18–60 keV) triggers of GRB-like events with a localization accuracy of 2–3 arcmin in the SA FoV ($\sim$1 sr) when operating in imaging mode.

Satellite data are currently transmitted to the ground on average every passage over the ASI Malindi ground station in Kenya and delivered to the *AGILE* Data Center (ADC; part of the ASI Space Science Data Center). Scientific data are then processed by a fast dedicated pipeline (*AGILE* GW, AGW), recently enhanced for the search of electromagnetic (EM) counterparts of GW sources. *AGILE* data processing can typically produce an alert for a transient gamma-ray source and/or GRB-like events within 20 minutes–2 hr from satellite

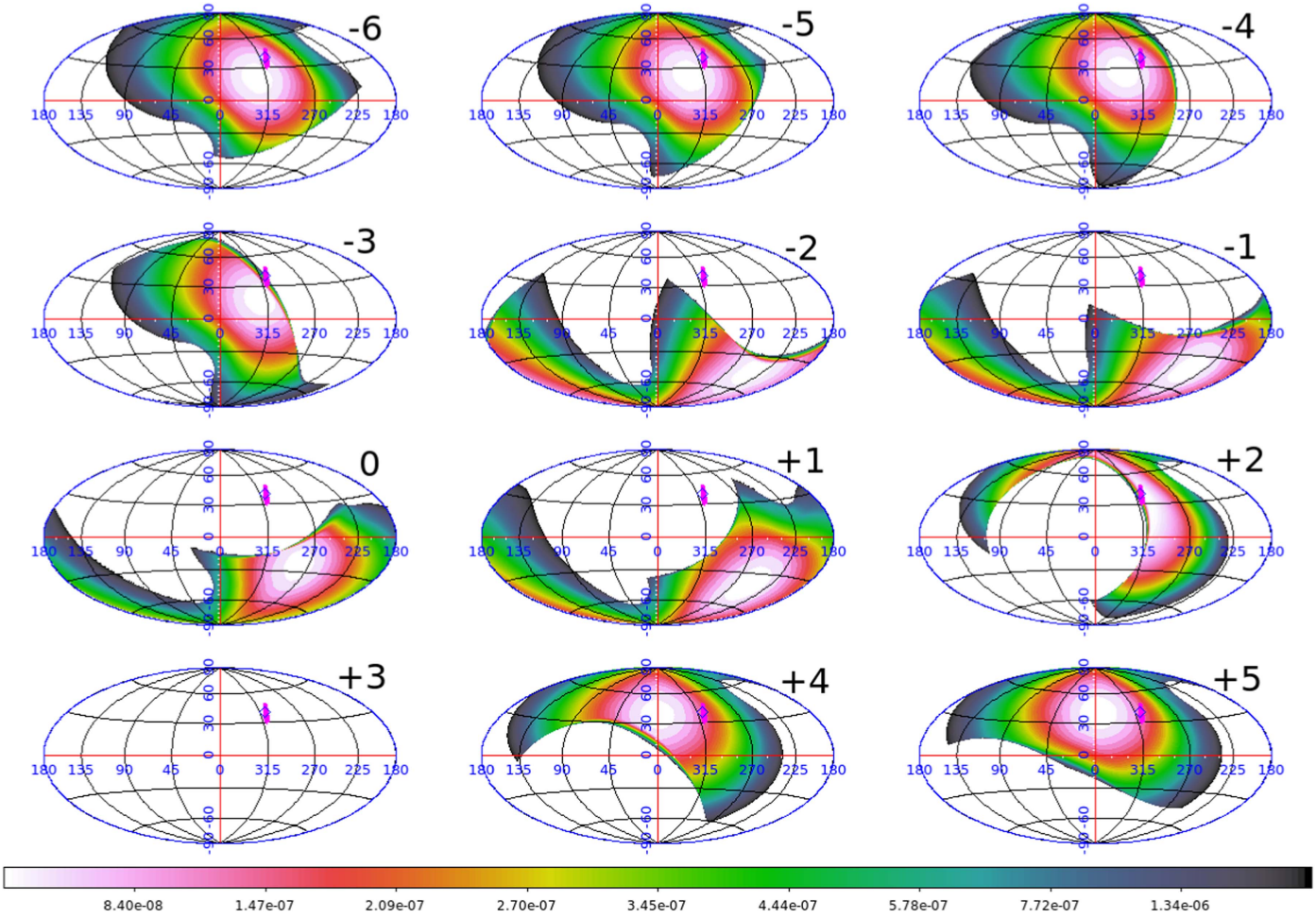

Figure 3. *AGILE*-GRID sequence of 12 passes over the OT AT 2017gfo obtained during the period (−2813 s, +2435 s) with respect to T_0. The maps report the gamma-ray flux 3σ upper limits (in erg cm^{-2} s^{-1}) in the energy range 30 MeV–10 GeV, with the lowest values at the OT AT 2017gfo position being UL $= 1.9 \times 10^{-8}$ erg cm^{-2} s^{-1}. The sequence shows all of the 150 s integration maps for all the single spinning rotations reported in Table 1. The magenta contour corresponds to the GW170817 LR according to the "preliminary LAL-inference" 90% c.l. (LIGO Scientific Collaboration & Virgo Collaboration 2017e), while the AT 2017gfo position is marked with the blue diamond symbol.

onboard acquisition depending on orbital and satellite parameters (Pittori 2013; Bulgarelli et al. 2014).

In this Letter, we present the main results of the analysis of *AGILE* data concerning GW170817. Section 2 presents the results on gamma-ray emission above 30 MeV from GW170817. Section 3 presents the results of SA, and MCAL observations. We discuss our measurements of GW170817 and their implications in Section 4.

2. Gamma-Ray Observations of GW170817

2.1. Prompt Emission

The *AGILE* satellite was occulted by the Earth at the moment of the LVC detection. Therefore, there are no prompt data obtained by the GRID at the position of the OT. Figure 1 shows the gamma-ray sensitivity map above 30 MeV at the GW170817 trigger time, with the Earth completely covering the GW170817 LR (obtained from the 90% LR extracted from the refined localization map; A17b). Since the *AGILE* satellite rotates every ∼7 minutes around the axis pointed toward the Sun, the GRID obtained exposures of the GW170817 LR for each satellite revolution not affected by Earth occultation or SAA passages. We consider here three types of time intervals preceding and following the T_0 with different integration timescales: (a) short timescales, with 150 s integrations covering the interval [−3100, +2900] s (times refer to T_0); (b) medium timescales, with integrations ranging from 1 hr to 1 day covering the interval [−1, +1] day; (c) long timescales, with integrations ranging from 1 day to 50 days covering the interval [−101, +21] days.

2.2. Early Observations with Short Timescales

For the relatively short exposures during the first passes of the GW170817 LR "GRB detection mode," that maximizes the detection of relatively short gamma-ray transients lasting a few tens of seconds (as already applied to the short GRB 090510; Giuliani et al. 2010). We show in Figure 3 the sequence of 150 s duration passes over the LR within $-3100\,\mathrm{s} < t < +2900\,\mathrm{s}$, and we summarize in Table 1 the 2σ flux UL obtained at the OT position. We label time intervals of the highest GRID exposure with progressive numbers with respect to the prompt interval ΔT_0. The intervals nearest in time to T_0 are the ΔT_{-3} and ΔT_{+2} ones. We then obtain 2σ flux ULs in the

Table 1
Analysis of Individual Passes over the OT Position in the GRB Detection Mode

Interval Number	Start Time[a] (s)	Δt[b] (s)	2σ UL 30 MeV–10 GeV[c] (10^{-8} erg cm^{-2} s^{-1})	Comments
−6	−2663	150	1.9	…
−5	−2213	150	1.9	…
−4	−1763	150	1.9	…
−3	−1335	150	54.5	…
−2	−1013	150	…	LVC source occulted by the Earth
−1	−563	150	…	LVC source occulted by the Earth
0	0	150	…	LVC source occulted by the Earth
+1	+335	150	…	LVC source occulted by the Earth
+2	+935	150	4.3	…
+3	+1385	150	…	excluded due to SAA passage
+4	+1835	150	2.4	…
+5	+2285	150	2.2	…
…	−3100	3100	0.6	…
…	+0	2900	0.5	…

Notes.
[a] Start time of the time interval with respect to T_0, $t - T_0$, in s.
[b] Integration time, in s.
[c] 2σ flux upper limit obtained with the "GRB detection mode" for emission at the AT 2017gfo position with integrations of 150 s except for the last two rows obtained with exposures of 3100 and 2900 s before and after T_0.

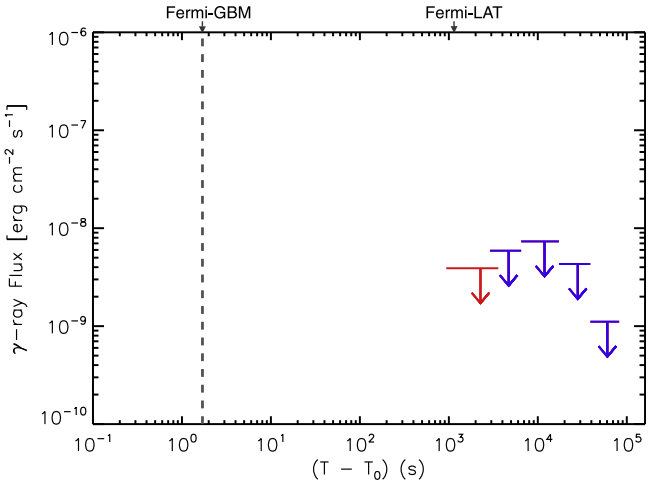

Figure 4. We show the *AGILE*-GRID gamma-ray 2σ ULs obtained at the AT 2017gfo position and at different times with integrations of 2665 s, marked in red color, and integrations ranging from 1 to 12 hr, marked in blue color.

30 MeV–10 GeV band, with 150 s integrations within the time interval [−3100, +2900] s.

The values for the integrations nearest in time to T_0 are (see Figure 2) $UL_{-3} = 5.5 \times 10^{-7}$ erg cm^{-2} s^{-1} for the interval [−1335, −1175] s and $UL_{+2} = 4.3 \times 10^{-8}$erg cm^{-2} s^{-1} for the interval [+935, +1085] s, the first one being obtained when the OT was near the Earth limb, so that the effective exposure is lower than that in other intervals. For a 2665 s integration including the ΔT_{+2} interval we obtain: $UL_{2\,ks} = 3.9 \times 10^{-9}$ erg cm^{-2} s^{-1} for the overall time interval[17] [+935, +3600] s. In Figure 4, we report our gamma-ray ULs obtained at the times reported in Table 1 with the indication of the GRB 170817A *Fermi*-GBM detection time and of the *Fermi*-LAT observation. No other gamma-ray observation of the GW170817 LR is available in the range 30 MeV–30 GeV.

Table 2
Analysis of GRID Data over Medium-timescale Integration Times at the OT Position

Interval Number	Start Time[a] (ks)	Δt[b] (hr)	2σ UL[c] (10^{-9} erg cm^{-2} s^{-1})
−10	−32.9	12	0.66
−9	−11.3	6	1.11
−8	−6.7	3	1.66
−7	−3.1	1	10.07
+6	+2.9	1	5.89
+7	+6.5	3	7.33
+8	+17.3	6	4.31
+9	+38.9	12	1.11
…	−86.4	24	0.55
…	+0	24	1.47

Notes.
[a] Start time of the interval with respect to T_0, $t - T_0$, in ks. The second table part reports the UL on integrations on the total time covering all the pre-/post-T_0 intervals.
[b] Integration time, in hr.
[c] 2σ flux upper limit (10^{-9} erg cm^{-2} s^{-1}) obtained for emission in the range 100 MeV–10 GeV with the *AGILE* maximum likelihood analysis at the AT 2017gfo position.

2.3. Search for Precursor and Delayed Gamma-Ray Emission

AGILE was uniquely able to collect data on the GW170817 LR during selected time intervals preceding and following the prompt event. We carried out a search for transient gamma-ray emission on integrations smaller than one day (see Table 2) during the hours and days immediately following or preceding the prompt event (see Figure 5). Finally, we also performed a search on longer timescales up to 100 days before and 20 days after the event. Table 3 summarizes our results and ULs for these long integrations. No significant gamma-ray emission in the GW170817 LR was detected over integrations of hours up to 50 days at covering times from $Ts_0 - 101$ days to $T_0 + 21$ days.

The long-timescale GRID data analysis included two further searches for transient gamma-ray detections with equal integrations of 1000 s, 12 hr, 1 day, and 2 days. In particular, we have performed a search for gamma-ray emission from 2017 August 1 to 31, at a 1000 s integration timescale. On 2017 August 24, 09:31:39 UTC, using the method described in Li & Ma (1983), we detected a weak gamma-ray source spatially coincident with the GW170817 OT at 4.2σ pre-trial significance. Our analysis leads to a marginal post-trial significance of 3.1σ for this source. Similar searches on 1 and 2 day integration

[17] The integration time of 2665 s corresponds to a lower effective exposure time of ∼400 s because of the satellite revolutions in spinning mode (see Table 1).

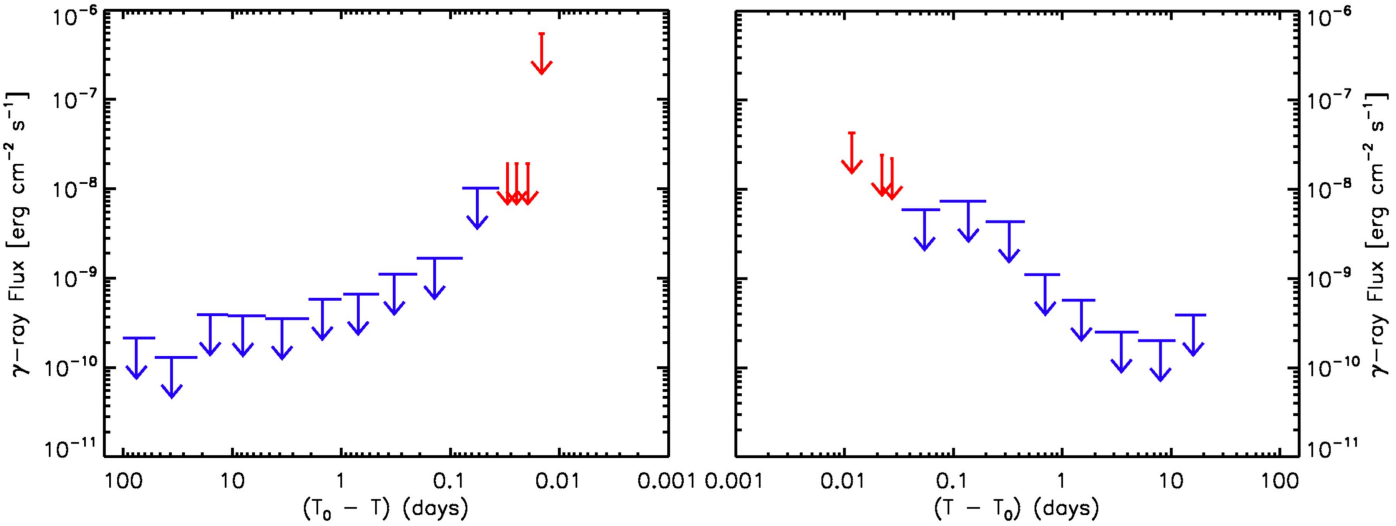

Figure 5. *AGILE*-GRID gamma-ray 2σ flux ULs obtained at the OT position at different times and integrations. Integrations of 150 s in the 30 MeV–10 GeV band are marked in red color, while those ranging from 1 hr to 100 days in 100 MeV–10 GeV are marked in blue color. On the left the ULs preceding T_0 till $T_0 - 101$ days, and on the right the ones following it until $T_0 + 21$ days.

Table 3
Long-timescale Integration Times Analysis at the OT Position

Interval Number	Start Time[a] (days)	Δt [b] (days)	2σ UL [c] (10^{-10} erg cm^{-2} s^{-1})
−16	−101	50	2.12
−15	−51	30	1.30
−14	−21	10	3.88
−13	−11	6	3.80
−12	−5	3	3.52
−11	−2	1	5.79
+10	+1	1	5.71
+11	+2	3	2.52
+12	+5	6	2.01
+13	+11	10	3.88

Notes.
[a] Start time of the interval with respect to T_0, $t - T_0$, in days.
[b] Integration time, in days.
[c] 2σ flux upper limit (10^{-10} erg cm^{-2} s^{-1}) obtained for emission in the range 100 MeV–10 GeV with the *AGILE* maximum likelihood analysis at the AT 2017gfo position and for a mean power-law spectrum with photon index −2.

timescales over [−10, +10] days time interval have been performed discarding low-exposure integrations and executing the *AGILE* maximum likelihood analysis (Mattox et al. 1996; Bulgarelli et al. 2012) at the OT position. Another low-significance source spatially coincident with the OT is found in a 1 day integration starting at August 9, 00:00:00 UTC, with a pre-trial significance of 3.3σ.

3. SA and MCAL Observations

The SA detector (Feroci et al. 2009) observed the location of GW170817 starting at 2017 August 18 01:16:34.84 UTC, that is, with a $\Delta t = 0.53$ days with respect to the LVC trigger time restarting its science observations after a 12 hr period of "idle mode," due to telemetry-saving requirements at mission level. We report here the analysis for the first available orbit after the idle time interval. The location of GW170817 thus crossed the FoV of the SA detector at 23.5° off-axis in one coordinate (*X*), while scanning the entire FoV in the orthogonal coordinate (*Y*). This is a rather unfavorable viewing angle for SA, greatly reducing its effective area and sensitivity thereof. We restricted our analysis between −15° and +15° in the *Y*-coordinate, exposing on average 32% of the peak effective area. The observation of the GW source is composed by a set of 15 time intervals (one per satellite rotation), each one lasting about 40 s, for a total net exposure time of 573 s. No X-ray source was detected at the location of GW170817, with a 3σ UL in the 18–60 keV energy band of 3.0 $\times 10^{-9}$ erg cm^{-2} s^{-1}.

As the OT is de-occulted and accessible by MCAL near +935 s, we obtain flux ULs with the MCAL detector at times −1328 s and +1023 s. No evidence of triggered or untriggered significant emission detected by MCAL was measured. We obtained a 2σ fluence UL in the energy band 400 keV–100 MeV, UL = 3.1 $\times$ 10^{-7} erg cm^{-2} at times −1328 s and +1023 s, using a power-law model with a photon index of 1.4.

4. Discussion and Conclusions

AGILE contributed in a significant way to the multi-frequency follow-up observations of the exceptional event GW170817 (MMA17). Despite the Earth occultation of the LR at T_0, *AGILE* obtained very relevant X-ray and gamma-ray constraints on GW170817. As reported in Bulgarelli et al. (2017) and MMA17, the earliest gamma-ray imaging detector data were obtained near $T_1 = +935$ s. Table 1 and Figure 3 show the results of the first useful passes over the GW170817 LR. Of particular relevance to our discussion is the upper limit to gamma-ray emission above 30 MeV obtained with an integration of about 2600 s after T_1, $F_\gamma = 3.9 \times 10^{-9}$erg cm^{-2} s^{-1}. For a distance $d = 40$ Mpc this translates into a limiting isotropic gamma-ray luminosity $L_{\mathrm{iso}_\gamma} = 7.8 \times 10^{44}$ erg s^{-1} in the range 30 MeV–10 GeV. It is interesting to note that the peak isotropic luminosity of GRB 170817A in the 10–1000 keV band detected by *Fermi*-GBM is $L_{\mathrm{iso,GBM}} \simeq 6 \times 10^{46}$ erg s^{-1} (Abbott et al. 2017e; Goldstein et al. 2017; MMA17). Figures 3 and 5 show the overall trend of the gamma-ray upper limits obtained by the

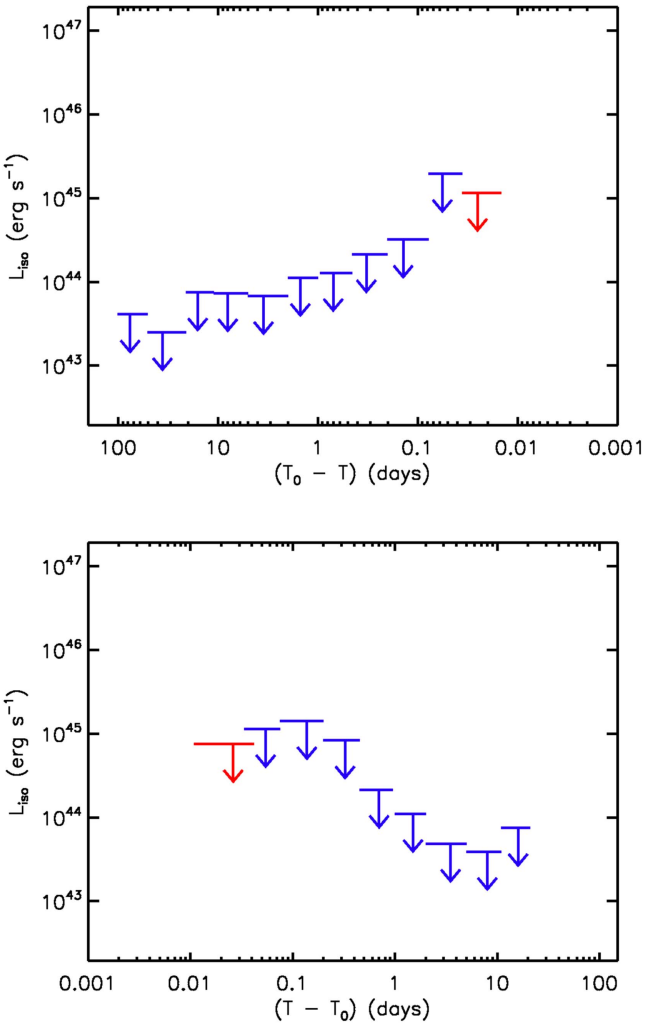

Figure 6. *AGILE*-GRID sequence of ULs converted into isotropic luminosity limits (in erg s^{-1}) assuming the OT distance of 40 Mpc. Top panel: data regarding the intervals preceding the NS–NS coalescence. The UL obtained in "GRB detection mode" for an integration of 1915 s in the 30 MeV–10 GeV band is marked in red. Bottom panel: flux ULs obtained for the intervals following the NS–NS coalescence. The UL obtained in "GRB detection mode" for an integration of 2665 s in the 30 MeV–10 GeV band is marked in red. In both panels, we show the ULs obtained with the ML analysis in the range 100 MeV–10 GeV in blue. All GRID ULs were obtained at the OT position.

AGILE-GRID at later times. In terms of upper limits of the gamma-ray luminosity, the results of Figure 6 indicate a range of isotropic luminosities between 10^{43} and 10^{45} erg s^{-1}. Furthermore, the imaging SA provided one of the earliest upper limits to hard X-ray emission in the band 18–60 keV at $\Delta t = 0.53$ days (see also Table 4 of MMA17), $F_X < 3 \times 10^{-9}$ erg cm^{-2} s^{-1}, which translates into a limiting isotropic luminosity of $L_{iso,X} = 5.8 \times 10^{44}$ erg s^{-1}. We note that both GRID and SA provide similar limits to the emitted luminosity in their different energy bands even though measured at different times (+0.011 days and +0.53 days, respectively). The non-imaging MCAL provided data as the GW170817 LR was de-occulted by the Earth. Assuming the same spectral model applicable to GRB 170817A (MMA17), the 90% c.l. fluence upper limit is $F_{MCAL} < 3 \times 10^{-7}$erg cm^{-2}, which turns out to be similar to other measurements by other calorimetric detectors (see Table 3 of MMA17).

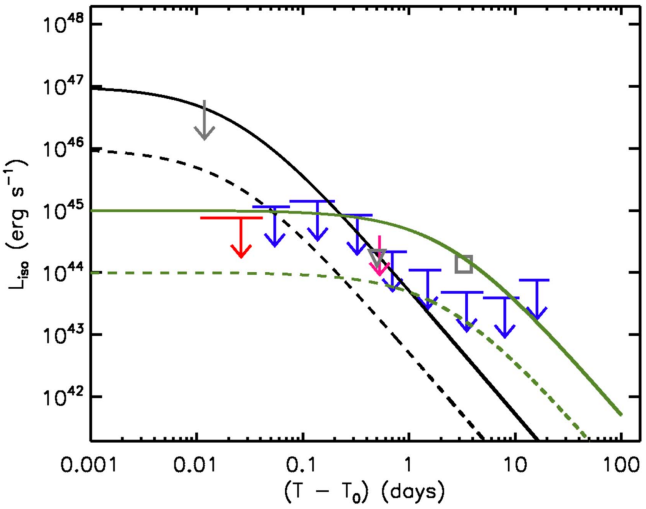

Figure 7. *AGILE* 2σ ULs obtained from observations of the GW170817 localization region and converted into luminosity limits (in erg s^{-1}) for an OT distance of 40 Mpc. We show the *AGILE*-GRID ULs in the energy range 100 MeV–10 GeV in blue. We show the early GRID UL in the range 30 MeV–10 GeV in red. Marked in magenta and gray are the SA and MCAL flux ULs in the 18–60 keV and 400 keV– 100 MeV bands, respectively. We mark by a gray triangle the post-merger UL *Fermi*-GBM (20–100 keV), and by a gray square the *INTEGRAL*-SPI (500–1000 keV) post-merger luminosity UL (MMA17). We also show the high-energy luminosity curves relative to the magnetar-like remnant model described in Section 4. The black lines refer to a model with a poloidal magnetic field $B_p = 10^{15}$ G and radiation efficiencies ξ of 10^{-2} (solid line) and 10^{-3} (dashed line). Green lines correspond to a model with $B_p = 10^{14}$ G and $\xi = 10^{-2}$ (solid) or $\xi = 10^{-3}$ (dashed).

The limiting luminosities implied by our measurements can be interpreted in a context of high-energy radiation possibly emitted by either an expanding fireball/jet or by a remnant left over from the NS–NS coalescence. The latter hypothesis is more interesting in terms of constraints that can be obtained by the *AGILE*-GRID observations. If the remnant is a magnetar-like system loaded with a residual magnetic field and rapidly rotating (e.g., Duncan & Thompson 1992; Usov 1992; Thompson 1994; Spruit 1999; Zhang & Meszaros 2001), we can constrain its magnetic field assuming initial millisecond spin periods. The electromagnetic emission (EM) by magnetic dipole radiation of a star of radius R with a poloidal magnetic field B_p and angular frequency $\Omega = 2\pi/P$ (with P as the spin period) is $L(t) = B_p^2 R^6 \Omega(t)^4/6c^3$ (with c as the speed of light). Neglecting GW radiation at late times after coalescence, integration of the energy loss equation leads to the dependence of Ω as a function of time, $\Omega(t) = \Omega_0(1 + t/\tau)^{-1/2}$, with Ω_0 as the initial frequency and $\tau = 3c^3 I/(B_p^2 R^6 \Omega_0^2) \simeq (2 \times 10^3$ s$) I_{45} B_{p,15}^{-2} P_{0,-3}^2 R_6^{-6}$, where I_{45} is the compact object moment of inertia in units of 10^{45} g cm^2, $B_{p,15} = B_p/10^{15}$ G, $P_{0,-3}$ is the initial spin period in units of 10^{-3} s, and R_6 is the radius of the compact object in units of 10^6 cm. For the EM-dominated regime of energy loss, we obtain the temporal behavior of the spin-down luminosity (e.g., Zhang & Meszaros 2001) $L_{sd}(t) = L_0/(1 + t/\tau)^2$, with $L_0 = I\,\Omega_0^2/(2\,\tau) \simeq (10^{49}$ erg s$^{-1}) B_{p,15}^2 P_{0,-3}^{-4} R_6^6$. It is interesting to note that in the absence of absorption effects, the radiated luminosity (in first approximation assumed here to be isotropic) has the limiting behaviors $L_{sd} = L_0$ for $t \ll \tau$ and $L_{sd} = L_0\,(t/\tau)^{-2}$ for $t \gg \tau$. In our case, we can assume the remnant of radius $R_6 = 1$ and moment of inertia $I_{45} = 1$ to rotate with an initial millisecond spin period, $P_{0,-3} = 1$. We

then have the critical time τ depending only on the surface magnetic field $\tau \simeq (2 \times 10^3 \text{ s}) B_{p,15}^{-2}$.

Assuming a conversion of spin-down luminosity $L_{\rm sd}(t)$ into radiation by a factor ξ, we show the radiated luminosity $L_{\rm rad}(t) = \xi L_{\rm sd}(t)$ in Figure 7 under the assumptions of two different values of the poloidal magnetic field $B_p = 10^{15}$ G and 10^{14} G, for two values of the conversion factors, $\xi = 10^{-2}$ and $\xi = 10^{-3}$. We denote by ξ the possibly different conversion efficiencies into hard X-rays and the GRID energy range above 30 MeV. We show in Figure 7 all the *AGILE* upper limits (from MCAL, SA, and GRID) together with the temporal behavior of high-energy radiation expected from a rapidly rotating magnetar, compared with the post-merger flaring UL from *Fermi*-GBM (20–100 keV) and *INTEGRAL*-SPI (500–1000 keV; MMA17) for integrations of 1 and 4.7 days, respectively. We see that the early *AGILE*-GRID upper limits are important in general and, in particular, exclude highly magnetized magnetars. We see in Figure 7 that magnetar models with $B_p = 10^{15}$ G are excluded by the earliest GRID upper limit with high confidence also for $\xi = 10^{-3}$. Analogously, models with $B_p = 10^{14}$ G are excluded for $\xi = 10^{-2}$.

Constraining the gamma-ray emission of GW170817 at early times (within the first few thousand seconds) is relevant also to models of possible magnetic field reconnection following the formation of a black hole. Transient gamma-ray emission can be expected from the collapse of the coalescing NSs into a newly born black hole. We exclude models envisioning gamma-ray luminosities near 10^{45} erg s^{-1} at +1000 s after coalescence.

AGILE continues to operate nominally and will continue to observe the high-energy sky in the search for transient events associated with gravitational-wave events.

This work is part of the multi-frequency observation campaign of GW170817, whose main results are summarized in the multi-messenger astronomy (MMA) paper. We warmly thank our LIGO–Virgo and MMA collaborators for sharing information on the event and follow-up observations. We thank the anonymous referee for valuable comments. *AGILE* is an ASI space mission developed with programmatic support by INAF and INFN. We thank INAF and ASI for support. We acknowledge partial support through the ASI grant No. I/028/12/2.

ORCID iDs

F. Verrecchia https://orcid.org/0000-0003-3455-5082
M. Tavani https://orcid.org/0000-0003-2893-1459
I. Donnarumma https://orcid.org/0000-0002-4700-4549
G. Piano https://orcid.org/0000-0002-9332-5319
C. Pittori https://orcid.org/0000-0001-6661-9779
A. Morselli https://orcid.org/0000-0002-7704-9553

References

Abbott, B. P., Abbott, R., Abbott, T. D., et al. 2016a, PhRvD, 93, 122003
Abbott, B. P., Abbott, R., Abbott, T. D., et al. 2016b, PhRvL, 116, 131103
Abbott, B. P., Abbott, R., Abbott, T. D., et al. 2016c, PhRvL, 116, 241103
Abbott, B. P., Abbott, R., Abbott, T. D., et al. 2016d, PhRvL, 116, 061102
Abbott, B. P., Abbott, R., Abbott, T. D., et al. 2016e, PhRvD, 93, 122004
Abbott, B. P., Abbott, R., Abbott, T. D., et al. 2016f, PhRvL, 116, 241102
Abbott, B. P., Abbott, R., Abbott, T. D., et al. 2017a, PhRvL, 118, 221101
Abbott, B. P., Abbott, R., Abbott, T. D., et al. 2017b, PhRvL, 119, 161101
Abbott, B. P., Abbott, R., Abbott, T. D., et al. 2017c, PhRvL, 119, 141101
Abbott, B. P., Abbott, R., Abbott, T. D., et al. 2017d, ApJL, 848, L12
Abbott, B. P., Abbott, R., Abbott, T. D., et al. 2017e, ApJL, 848, L13
Acernese, F., et al. (Virgo Collaboration) 2015, CQGra, 32, 024001
Alexander, K., Berger, E., Fong, W., et al. 2017a, ApJL, 848, L21
Alexander, K. D., Fong, W., Berger, E., et al. 2017b, GCN, 21545
Allam, S., Annis, J., Berger, E., et al. 2017, GCN, 21530
Arcavi, I., Hosseinzadeh, G., Howell, D. A., et al. 2017b, Natur, 551, 64
Arcavi, I., Howell, D. A., McCully, C., et al. 2017a, GCN, 21538
Arcavi, I., Howell, D. A., McCully, C., et al. 2017c, ApJL, 848, L33
Balasubramanian, A., Mate, S., Bhalerao, V., et al. 2017, GCN, 21514
Bulgarelli, A., Chen, A. W., Tavani, M., et al. 2012, A&A, 540, A79
Bulgarelli, A., Tavani, M., Verrecchia, F., et al. 2017, GCN, 21564
Bulgarelli, A., Trifoglio, M., Gianotti, F., et al. 2014, ApJ, 781, 19
Connaughton, V., Blackburn, L., Briggs, M. S., et al. 2017, GCN, 21506
Coulter, D. A., Foley, R. J., Kilpatrick, C. D., et al. 2017b, Sci, https://doi.org/10.1126/science.aap9811
Coulter, D. A., Kilpatrick, C. D., Siebert, M. R., et al. 2017a, GCN, 21529
Cowperthwaite, P. S., et al. 2017, ApJL, 848, L17
Del Monte, E., Barbiellini, G., Donnarumma, I., et al. 2011, A&A, 535, A120
Drout, M. R., Piro, A. L., Shappee, B. J., et al. 2017, Sci, https://doi.org/10.1126/science.aaq0049
Duncan, R. C., & Thompson, C. 1992, ApJL, 392, L9
Evans, P., Cenko, B., Kennea, J. A., et al. 2017a, Sci, https://doi.org/10.1126/science.aap9580
Evans, P., Cenko, B., Kennea, J. A., et al. 2017b, GCN, 21612
Feroci, M., Costa, E., Soffitta, P., et al. 2009, NIMPA, 598, 470
Fong, W., Margutti, R., Haggard, D., et al. 2017, GCN, 21786
Fuschino, F., Labanti, C., Galli, M., et al. 2008, NIMPA, 588, 17
Galli, M., Marisaldi, M., Fuschino, F., et al. 2013, A&A, 553, A33
Giuliani, A., Fuschino, F., Vianello, G., et al. 2010, ApJL, 708, L84
Giuliani, A., Longo, F., Verrecchia, F., et al. 2013, GCN, 15479
Giuliani, A., Mereghetti, S., Fornari, F., et al. 2008, A&A, 491, L25
Giuliani, A., Mereghetti, S., Marisaldi, M., et al. 2014, arXiv:1407.0238
Goldstein, A., Veres, P., Burns, E., et al. 2017, ApJL, 848, L14
Harrison, F. A., Forster, K., Garcia, J., et al. 2017, GCN, 21626
Kasliwal, M., Nakar, E., Singer, L. P., & Kaplan, D. E. A. 2017, Sci, doi:10.1126/science.aap9455
Kocevski, D., Omodei, N., Buson, S., et al. 2017, GCN, 21534
Labanti, C., Marisaldi, M., Fuschino, F., et al. 2009, NIMPA, 598, 470
Li, T., & Ma, Y. 1983, ApJ, 272, 317
Li, T. P., Xiong, S. L., Zhang, S. N., et al. 2017, SCPMA, doi:10.1007/s11433-017-9107-5
Liao, J. Y., Li, C. K., Ge, M. Y., et al. 2017, GCN, 21518
LIGO Scientific Collaboration & Virgo Collaboration 2017a, GCN, 21505
LIGO Scientific Collaboration & Virgo Collaboration 2017b, GCN, 21509
LIGO Scientific Collaboration & Virgo Collaboration 2017c, GCN, 21510
LIGO Scientific Collaboration & Virgo Collaboration 2017d, GCN, 21513
LIGO Scientific Collaboration & Virgo Collaboration 2017e, GCN, 21527
Lipunov, V. M., Gorbovskoy, E., Kornilov, V. G., et al. 2017a, ApJL, 850, L1
Lipunov, V. M., Gorbovskoy, E., Kornilov, V. G., et al. 2017b, GCN, 21546
Longo, F., Giuliani, A., Marisaldi, M., et al. 2013, GCN, 14344
Longo, F., Moretti, E., Nava, L., et al. 2012, A&A, 547, A95
Margutti, R., Berger, E., Fong, W., et al. 2017b, ApJL, 848, L20
Margutti, R., Fong, W., Berger, E., et al. 2017a, GCN, 21648
Marisaldi, M., Labanti, C., Fuschino, F., et al. 2008, A&A, 490, 1151
Mattox, J. R., Bertsch, D. L., Chiang, J., et al. 1996, ApJ, 461, 396
Melandri, A., Campana, S., Covino, S., et al. 2017, GCN, 21532
Nakahira, S., Yoshida, A., Sakamoto, T., et al. 2017, GCN, 21641
Pian, E., D'Elia, V., Piranomonte, F., et al. 2017b, GCN, 21592
Pian, E., D'Avanzo, P., Benetti, S., et al. 2017a, Natur, 551, 67
Piano, G., Verrecchia, F., Pilia, M., et al. 2017, GCN, 21526
Pilia, M., Cardillo, C., Piano, G., et al. 2017, GCN, 21525
Pittori, C. 2013, NuPhS, 239, 104
Savchenko, V., Ferrigno, C., Kuulkers, E., et al. 2017b, GCN, 21672
Savchenko, V., Mereghetti, S., Ferrigno, C., et al. 2017a, GCN, 21507
Singer, L. P., Lau, R., Kasliwal, M. M., et al. 2017, GCN, 21552
Singer, L. P., & Price, L. R. 2016, PhRvD, 93, 024013
Spruit, H. C. 1999, A&A, 341, L1
Sugita, S., Kawai, N., Serino, M., et al. 2017, GCN, 21555
Svinkin, D., Golenetskii, S., Aptekar, R., et al. 2017, GCN, 21746
Tanvir, N. R., Levan, A. J., González-Fernández, C., et al. 2017b, ApJL, 848, L27
Tanvir, S., Levan, S., et al. 2017a, GCN, 21544
Tavani, M., Barbiellini, G., Argan, A., et al. 2009, A&A, 502, 995
Tavani, M., Pittori, C., Verrecchia, F., et al. 2016, ApJL, 825, L4
Thompson, C. 1994, MNRAS, 270, 480
Troja, E., Piro, L., Sakamoto, T., et al. 2017b, GCN, 21765
Troja, E., Piro, L., van Eerten, H., et al. 2017a, Natur, 551, 71

Usov, V. V. 1992, Natur, 357, 472
Valenti, S., Sand, D. J., Yang, S., et al. 2017, ApJL, 848, L24
Veitch, J., Raymond, V., Farr, B., et al. 2015, PhRvD, 91, 042003
Verrecchia, F., Cardillo, M., Bulgarelli, A., et al. 2017, GCN, 21785
Verrecchia, F., Pittori, C., Giuliani, A., et al. 2013, GCN, 14515
von Kienlin, A., Meegan, C., Goldstein, A., et al. 2017, GCN, 21520
Yang, S., Valenti, S., Sand, D., et al. 2017, GCN, 21531
Zhang, B., & Meszaros, P. 2001, ApJL, 552, L35